

Video Article

Solid-state Graft Copolymer Electrolytes for Lithium Battery Applications

Qichao Hu¹, Antonio Caputo², Donald R. Sadoway¹¹Materials Science and Engineering, Massachusetts Institute of Technology²Materials Processing Center, Massachusetts Institute of TechnologyCorrespondence to: Qichao Hu at qichaohu@mit.eduURL: <http://www.jove.com/video/50067>DOI: [doi:10.3791/50067](https://doi.org/10.3791/50067)Keywords: Materials Science, Issue 78, Physics, Chemistry, Chemical Engineering, Chemistry and Materials, Engineering, Lithium Batteries, Polymer Electrolytes, Polyethylene oxide, Graft Copolymer, LiFePO₄, synthesis, polymers

Date Published: 8/12/2013

Citation: Hu, Q., Caputo, A., Sadoway, D.R. Solid-state Graft Copolymer Electrolytes for Lithium Battery Applications. *J. Vis. Exp.* (78), e50067, doi:10.3791/50067 (2013).

Abstract

Battery safety has been a very important research area over the past decade. Commercially available lithium ion batteries employ low flash point (<80 °C), flammable, and volatile organic electrolytes. These organic based electrolyte systems are viable at ambient temperatures, but require a cooling system to ensure that temperatures do not exceed 80 °C. These cooling systems tend to increase battery costs and can malfunction which can lead to battery malfunction and explosions, thus endangering human life. Increases in petroleum prices lead to a huge demand for safe, electric hybrid vehicles that are more economically viable to operate as oil prices continue to rise. Existing organic based electrolytes used in lithium ion batteries are not applicable to high temperature automotive applications. A safer alternative to organic electrolytes is solid polymer electrolytes. This work will highlight the synthesis for a graft copolymer electrolyte (GCE) poly(oxyethylene) methacrylate (POEM) to a block with a lower glass transition temperature (T_g) poly(oxyethylene) acrylate (POEA). The conduction mechanism has been discussed and it has been demonstrated the relationship between polymer segmental motion and ionic conductivity indeed has a Vogel-Tammann-Fulcher (VTF) dependence. Batteries containing commercially available LP30 organic (LiPF₆ in ethylene carbonate (EC):dimethyl carbonate (DMC) at a 1:1 ratio) and GCE were cycled at ambient temperature. It was found that at ambient temperature, the batteries containing GCE showed a greater overpotential when compared to LP30 electrolyte. However at temperatures greater than 60 °C, the GCE cell exhibited much lower overpotential due to fast polymer electrolyte conductivity and nearly the full theoretical specific capacity of 170 mAh/g was accessed.

Video Link

The video component of this article can be found at <http://www.jove.com/video/50067/>

Introduction

Lithium (Li) is a highly electropositive metal (-3.04 V relative to standard hydrogen electrode), and the lightest metal (equivalent weight of 6.94 g/mol and specific gravity of 0.53 g/cm³). This makes it attractive as a choice for the active material in the negative electrode and ideal for portable energy storage devices where size and weight matter. **Figure 1** shows that lithium-based batteries (Li ion, PLiON, and Li metal) have higher energy densities than lead-acid, nickel-cadmium, and nickel-metal-hydride batteries¹.

A full lithium-ion battery consists of a cathode (positive), an anode (negative), an electrolyte, and a separator (**Figure 2**). Both the cathode and the anode are intercalation compounds, where Li-ions can intercalate or de-intercalate reversibly (if the anode is carbon, Li intercalates as neutral Li). The electrolyte provides ionic conduction and insulates electronic conduction between the electrodes. The separator is permeable to ions, but mechanically rigid to keep the two electrodes from shorting. When the cell is in a fully charged state all of the Li has intercalated in the anode, and when the cell is in a fully discharged state all of the Li-ions are intercalated in the cathode. During the spontaneous reaction, discharging electrons flow from the anode to the cathode through an external circuit to power a device, while the ions flow from the anode to the cathode through the electrolyte. The ions and electrons recombine at the cathode to maintain charge neutrality. Upon charging, the flow is reversed.

Most Li-ion battery development to date has focused on cathode materials because they determine the energy density of the battery rather than on the electrolyte, which has remained mostly the same for decades. The electrolyte is a key piece of the battery since it affects the overall power capability due to impedance both through the electrolyte itself and at the electrode-electrolyte interfaces.

The electrolyte used in Li-ion batteries generally consists of a salt of the type LiX and a non-aqueous solvent. Compared to the aqueous electrolytes used in other electrochemical systems, the disadvantages of Li-ion electrolytes are lower conductivity, higher cost, flammability, and environmental problems. Advantages include a wide temperature range (over which the electrolyte remains a liquid) from -150 °C to 300 °C, a wide voltage window (up to 5 V versus Li/Li⁺), and better compatibility with electrodes (aqueous electrolyte would react violently with Li metal and form LiOH and hydrogen)^{2, 3, 4-6}.

The main non-aqueous electrolytes used in batteries include organic carbonate-based liquids, polymers, ionic liquids, and ceramics. These electrolytes need to meet certain benchmarks to be used in practical Li-ion batteries. They include a conductivity of at least 10 mS/cm, a large

electrochemical window (>4.5 V for high voltage cathodes), low vapor pressure, good thermal and chemical stability, low toxicity, and low cost. For certain stringent applications such as the electric vehicles, all of these benchmarks must be met over a wide temperature range, typically from -20 °C to 60 °C. Since the focus of this work is on organic and polymer electrolytes, the remainder of this paper will focus on these electrolytes.

Carbonate based electrolytes consist of a lithium salt dissolved in an organic solvent. However, it is difficult for any one solvent to meet all of the requirements. For example, solvents with low vapor pressure, such as ethylene carbonate (EC) and propylene carbonate (PC), tend to have higher viscosities, leading to lower conductivity. Also EC is a solid at room temperature; this requires it to be combined with another solvent. Generally the electrolyte is a combination of several solvents. The common solvents and some of their physical properties are listed in **Table 1**.

Name	Melting Temperature (°C)	Boiling Temperature (°C)	Viscosity (mPa*s)
Dimethyl Carbonate (DMC)	4.6	90	0.5902 (25 °C)
Diethyl Carbonate (DEC)	-43	126.8	0.7529 (25 °C)
Ethylene carbonate (EC)	36.5	238	1.9 (40 °C)
Propylene Carbonate (PC)	-54.53	242	2.512 (25 °C)

Table 1. Common Carbonate Solvents ⁷.

Safer alternates to organic electrolytes are polymer based electrolytes. Polymer electrolytes are thin-films, non-volatile, non-flammable, and their flexibility allows them to be rolled and printed on a large commercial scale. Wright, *et al.* first demonstrated ion conduction in poly(ethylene oxide)-salt complexes (PEO) in 1973. It was later discovered that the safety concern associated with dendrite growth on Li metal in liquid electrolyte could be resolved by using PEO-based solid polymer electrolyte, which suppressed the growth of dendrites ⁸⁻¹⁷. There are three main types of polymer electrolytes: (1) solvent free dry solid polymer, (2) gel electrolytes, and (3) plasticized polymer, with a solvent free dry synthesis used in our work.

This paper will discuss (a) the solvent free dry polymer synthesis, (b) the polymer conduction mechanism, and (c) provide temperature cycling for both solid polymer and organic electrolytes.

Protocol

1. Graft Copolymer Synthesis ¹⁸⁻¹⁹

1. Synthesize the graft copolymers (POEM-g-PDMS and POEA-g-PDMS at 70:30 weight ratio) using a free radical polymerization approach by mixing 26 ml of POEM (or POEA) monomers (**Figure 3**), 12 ml of PDMS macromonomers, and 12 mg of 2,2'-Azobis(2-methylpropionitrile) (AIBN) (monomer:initiator [825:1]) in 160 ml of EA.
2. Seal the flask containing the clear solution with a rubber septum and purge with ultra high purity argon for 45 min.
3. Heat the solution to 72 °C (AIBN has a decomposition rate of $3.2 \times 10^{-5} \text{ sec}^{-1}$) in an oil bath under constant stirring for 24 hr.
4. The initially clear solution typically became visibly milky within 2 hr. Precipitate the final solution in an immiscible solvent, PE. Dry the polymer at 80 °C under less than 5 mTorr vacuum for 5 days to remove the residual moisture.
5. It was found that if the polymer were not dried properly, the excessive moisture would lead to crack formation when the polymer was casted into thin films.
6. The final graft copolymer (shown in **Figure 4**) had a molecular weight of 500,000 g/mol using gel permeation chromatography with polystyrene calibration standard.
7. Complex the graft copolymer with LiTFSI at a Li:EO ratio of 1:20 (1 g of POEM-g-PDMS (70:30) with 170 mg of LiTFSI) in a common solvent of THF to form the electrolyte.

2. Preparation of Composite Cathode

1. Synthesize the cathode by mixing ball-milled LiFePO₄ powders (Linyi Gelon New Battery Materials) and carbon black (Super P), and dissolving the mixture in GCE solution at a weight ratio of 5:1:1.
2. Heat the slurry to 80 °C (open-cap) while being stirred. Next sonicate the slurry by magnetically stirring to ensure proper mixing. Doctor-blade onto aluminum foil at a loading factor of 10 mg/cm² onto the aluminum foil to ensure better lamination to the aluminum.
3. Dry the composite cathode in a vacuum oven at 80 °C O/N to remove the residual THF and moisture.

3. Coin Cell Preparation and Testing

1. Transport the composite cathode into an argon-filled glovebox, and punch into small discs (area = 1.4 cm²) using a high-precision electrode cutter EL-CUT (EL-CELL). Drop cast pure GCE solution (POEM-g-PDMS, LiTFSI, both dissolved in THF) onto the electrode discs to form the electrolyte layer.
2. Heat the final cathode-electrolyte discs on a hot plate inside the glovebox with a dew point of -80 °C to evaporate the THF, and assemble into CR2032 coin cells along with equal-sized GCE-coated metallic lithium discs (Sigma-Aldrich, 0.75 mm thick) using a manual closing tool (Hohsen). The cell schematic is shown in **Figure 5**, where the gray particles represent LiFePO₄, the black particles represent carbon, the blue "spaghetti" represents the GCE, and the anode is lithium metal.
3. Assemble a second set of cells comprised of the same LiFePO₄ powders and lithium metal anode, but instead use PVDF binder resin (Kynar), PVDF separator (Celgard), and liquid electrolyte of 1 M LiPF₆ in EC:DMC at 1:1 ratio (LP30, Merck), to compare the performance.

- All assembly was done in a glovebox with a dew point of $-80\text{ }^{\circ}\text{C}$. A 32-channel MACCOR 4000 battery tester was used for the cycling tests at ambient temperature.

4. Polymer Conduction Mechanism

- The PEO segmental motions are typically associated with the torsion around C-C and C-O bonds. The semi-random segmental motion assists ion conduction by forming and breaking coordination sites for the solvated ions and providing free volume for the ions to diffuse under the influence of the electric field. The onset of the segmental motion occurs in the vicinity of the glass transition temperature, T_g , and becomes more facile as the temperature increases further beyond the T_g . At higher temperatures, local voids are produced by the polymer expansion, allowing polymer segments to move into the free volume¹⁹.
- Since the segmental motion is far more rapid in the amorphous phase above the T_g than in the crystalline phase, ion transport in polymer occurs predominantly in the amorphous phase. However, recently Li^+ conduction in crystalline $(\text{PEO})_6:\text{LiAsF}_6$ was demonstrated, although the conductivity is more than two orders of magnitude lower than in amorphous PEO. The crystalline or amorphous phase of the PEO/salt complex depends on the composition, temperature, and preparation method²⁰⁻²².
- Unlike in liquid, where ions move with their solvent sheath intact and transport is related to the macroscopic viscosity of the solvent; in solid polymer, where the polymer chains are increasingly entangled and cannot move over long distances, the ion transport is related to the microscopic viscosity of the segments of the polymer chains. The transport of ions along polymer chains needs to overcome two activation barriers, both are shown in **Figures 6** and **7**. One is the solvation of the ions by the coordinating EO units. This process involves the forming and breaking of chemical bonds, has Arrhenius dependence, and the conductivity is given by

$$\sigma A^{(E_a/kT)}$$

where σ is the conductivity, A is a constant, and E_a is the activation energy associated with the bonds. Because ions must dissociate from the coordination sites in order to move in the solid polymer, if the bonds are too strong, the cations become immobile. The cation-polymer bonds need to be strong enough for salt dissolution, but weak enough to allow for cation mobility.

- The transport of ions is from one coordination site to another. This process is related to the segmental motion of the polymer, has Vogel-Tammann-Fulcher (VTF) dependence²²⁻²⁵, and the conductivity is where T_0 is a reference temperature generally chosen to be 50 K below T_g . This equation suggests that thermal motion above T_0 contributes to transport process, and faster motion is expected for polymer with low T_g . The VTF process is related to the T_g , thus rate-limiting at low temperatures. At high temperatures, the segmental motion becomes facile enough that the Arrhenius process becomes rate limiting.

Representative Results

The room temperature cell cycling performance is shown in **Figure 8**. The left plot shows the charge and discharge profiles of cells with conventional liquid electrolyte (LP30) at 15 mA/g, and GCE/binder at 10 mA/g. **Figure 9** shows the discharge voltage profiles of the solid polymer cells at room temperature, $60\text{ }^{\circ}\text{C}$, and $120\text{ }^{\circ}\text{C}$ using a low current of 0.05 C. The discharge voltage profiles as functions of specific capacity are shown in **Figure 10**, where the discharge current is in μA and labeled next to the discharge curve. **Figure 10** shows poor rate capability at room temperature and much better rate capability at elevated temperatures. The energy densities (integrating the discharge voltage with respect to specific capacity) at different power densities (multiplying the constant current with discharge voltage) are shown in the Ragone plot in **Figure 11** for the different temperatures.

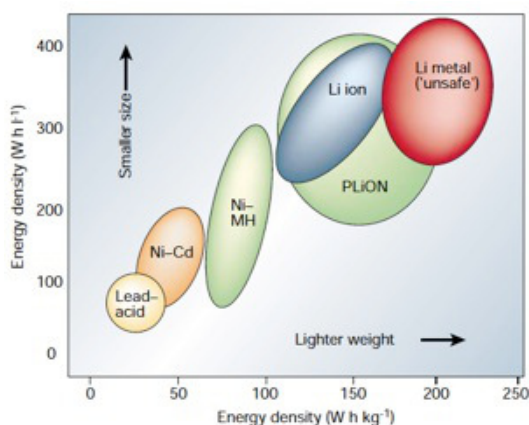


Figure 1. Energy densities for various batteries¹.

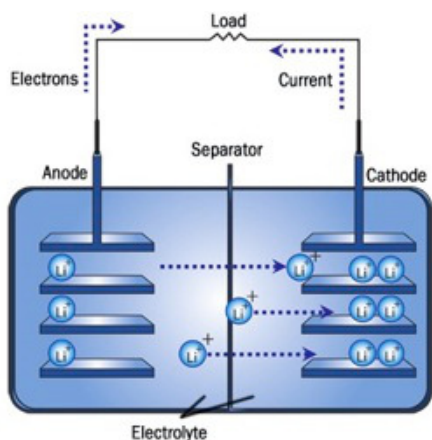
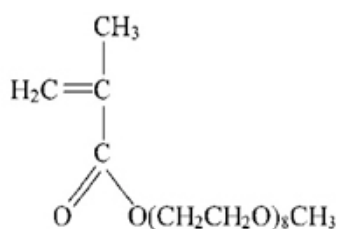
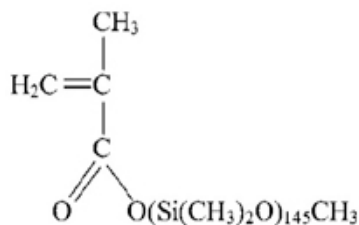


Figure 2. A full lithium-ion cell during discharging.



POEM monomer



PDMS macromonomer

Figure 3. POEM and PDMS.



Graft Copolymer

Figure 4. The Synthesized Graft Copolymer.

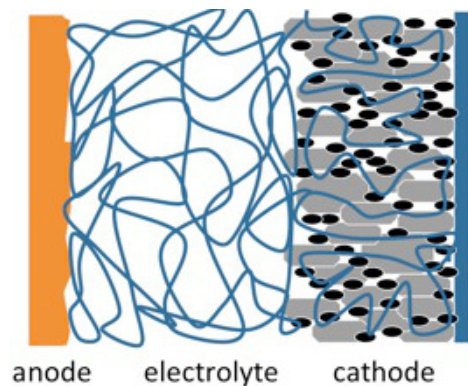


Figure 5. Schematic of a solid polymerlithium battery.

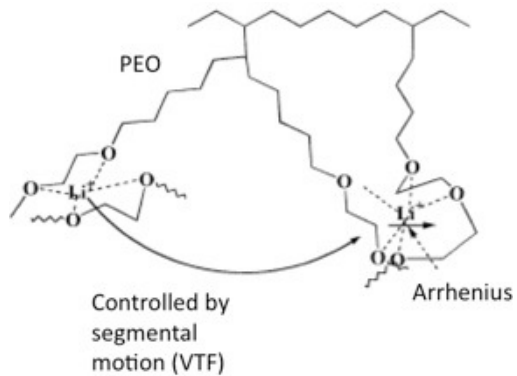


Figure 6. Contributions to ion mobility¹⁸.

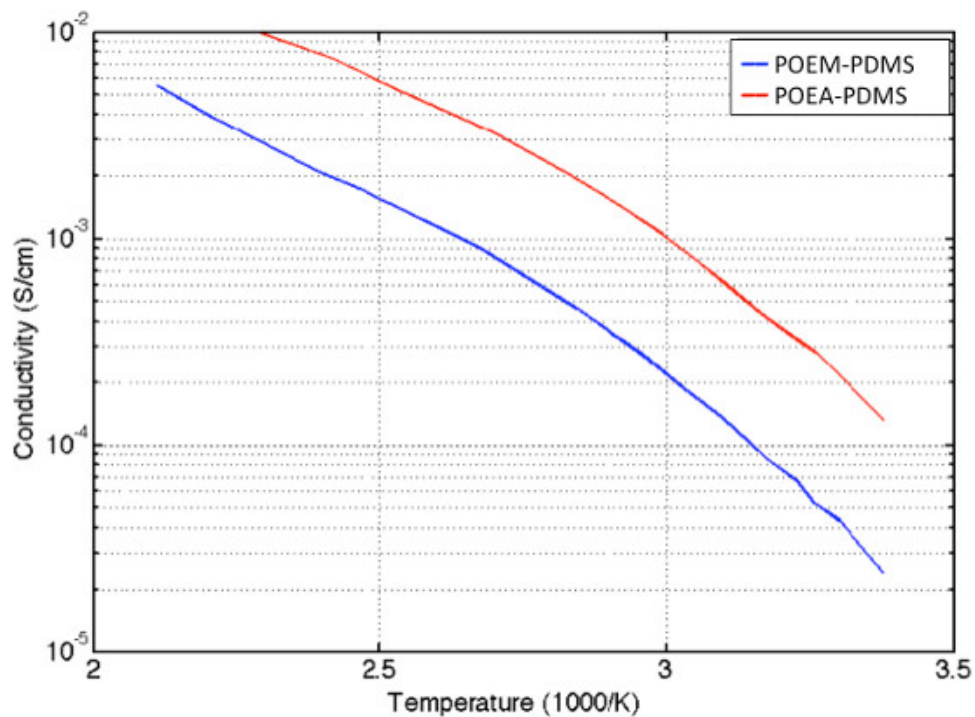


Figure 7. Conductivity of POEM and POEA at different temperatures.

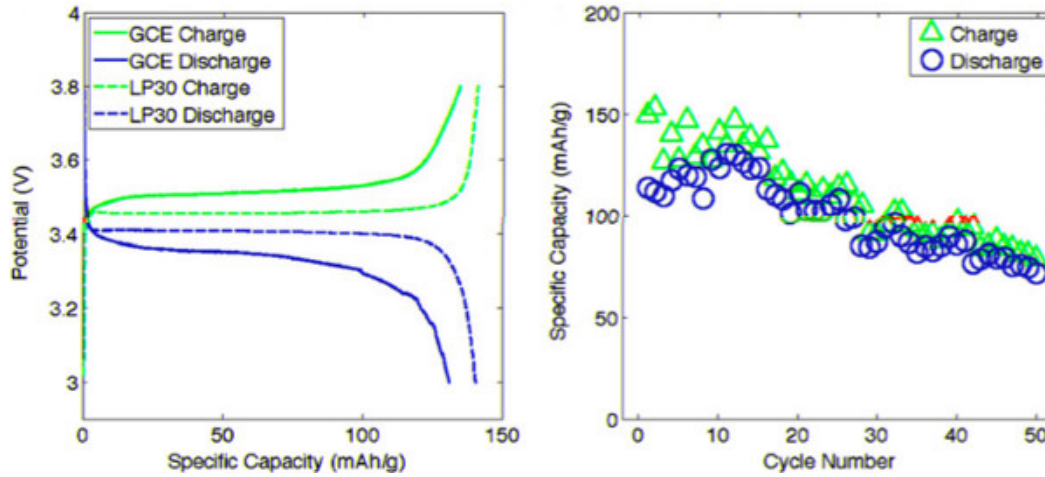


Figure 8. Room Temperature Cycling²⁶.

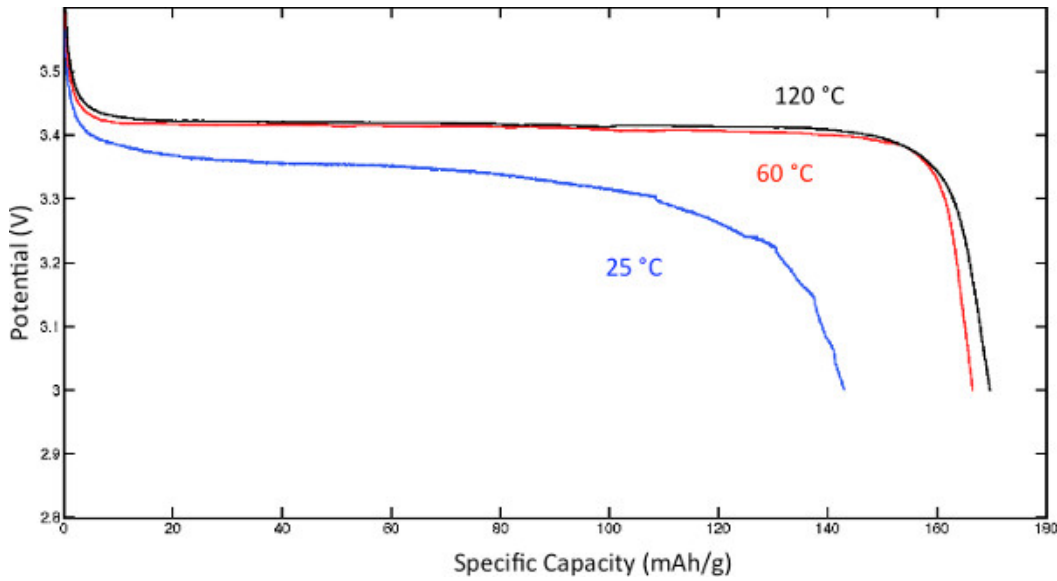


Figure 9. Discharge voltage profiles at different temperatures. [Click here to view larger figure.](#)

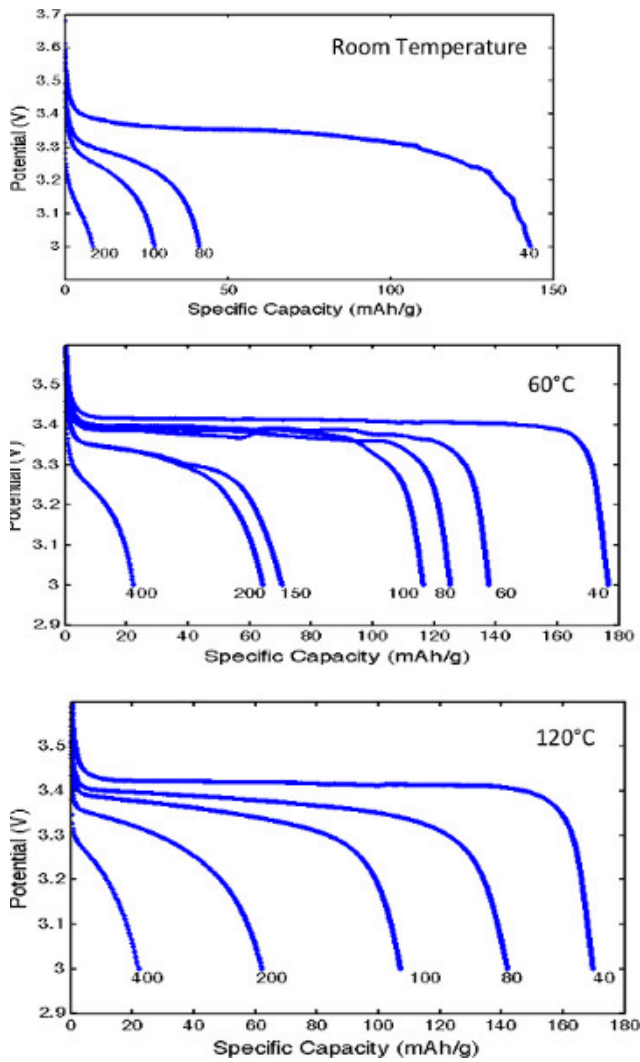


Figure 10. Discharge rate capability at different temperatures. [Click here to view larger figure.](#)

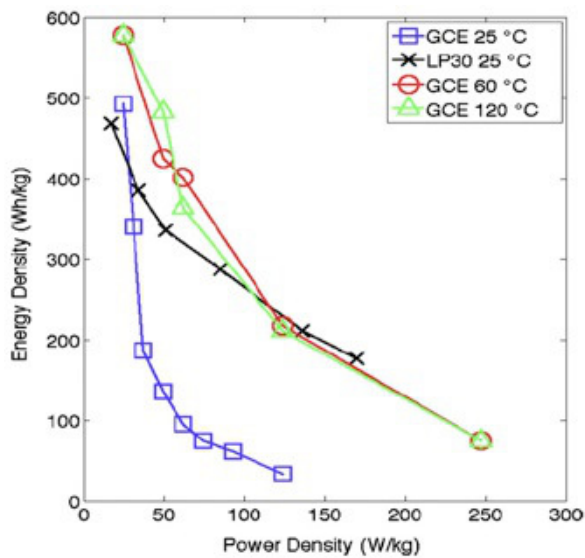


Figure 11. Ragone plot for polymer and liquid electrolyte batteries at different temperature²⁶.

Table 1. Common Carbonate Solvents.**List of Acronyms**

2,2'-Azobis(2-methylpropionitrile) (AIBN)

Graft copolymer electrolyte (GCE)

Diethyl carbonate (DEC)

Dimethyl carbonate (DMC)

Ethylene oxide (EO)

Ethylene carbonate (EC)

Ethyl acetate (EA)

Glass transition temperature (T_g)

Lithium hexafluorophosphate (LiPF_6)

LP30 (LiPF_6 in EC:DMC at a 1:1 ratio)

Lithium iron phosphate (LiFePO_4)

Lithium Hexafluoroarsenate (LiAsF_6)

Lithium bis(trifluoromethane)sulfonamide (LiTFSI)

Petroleum ether (PE)

Polydimethylsiloxane (PDMS)

Poly(oxyethylene) methacrylate (POEM)

Poly(oxyethylene) acrylate (POEA)

Propylene carbonate (PC)

Polyvinyl difluoride (PVDF)

Tetrahydrofuran (THF)

Vogel-Tammann-Fulcher (VTF)

Discussion

The $\text{LiFePO}_4/\text{GCE}/\text{Li}$ curves show greater overpotential than the $\text{LiFePO}_4/\text{LP30}/\text{Li}$ curves on both charge and discharge. Since the GCE is used as both electrolyte and binder, ion conduction is provided to all of the cathode particles, and nearly the entire practical specific capacity (150 mAh/g) was accessible. The theoretical specific capacity of 170 mAh/g is not achieved since it is limited by lithium diffusion within LiFePO_4 particles, which is low at room temperatures. The cycling capacities for the first 50 deep cycles are shown in the right plot. The energy efficiencies during the first 5 cycles are low (large charge/discharge capacity ratio), possibly due to the reversible capacity loss related to the formation of a passivation layer on lithium anode. The passivation film could result from reactions between lithium metal and residual THF solvent of the CF_3SO_3^- anions, which are known to produce LiF species.

At both 60 °C and 120 °C, the cell exhibits low overpotential due to fast polymer electrolyte conductivity, and nearly the full theoretical specific capacity can be accessed. Full rate capability test of the solid polymer cells were also performed at these three temperatures. At each temperature, the cells were charged at a constant current of 0.05 C (or 25 W/kg considering the cathode loading mass density) and discharged at higher currents. Fresh cells were used for each discharge current to isolate the effect of capacity fade. The rate capability test of a cell with commercial liquid electrolyte (LP30) was also performed at room temperature. The energy densities (integrating the discharge voltage with respect to specific capacity) at different power densities (multiplying the constant current with discharge voltage) are shown in the Ragone plot in **Figure 11** for the different temperatures. **Figure 11** reflects the tradeoff between energy density and power density. At large currents, the cell performance becomes diffusion limited and the cell capacity decreases. For the LP30-based cells, only room-temperature data were collected. In the case of the GCE-based cells, performance near 60 °C is of particular interest since this temperature is in the range of the melting point of PEO. As indicated in **Figure 11** at room temperature the energy densities of the GCE and LP30-based cells are comparable at low power densities. As the power density is increased from 25 to 50 W/kg, the energy density of the GCE-based cells falls drastically. However, at elevated temperatures (>60 °C), the decrease in energy density of the GCE-based cells with increasing power density is significantly smaller due to the

higher mobility of PEO chains. Above 60 °C, the performance of the GCE-based cell becomes less dependent on temperature and comparable to the room-temperature performance of the liquid electrolyte-based cells.

Disclosures

No conflicts of interest declared.

Acknowledgements

The authors would like to thank Weatherford International for providing financial support.

References

1. Tarascon, J.M. & Armand, M. Issues and challenges facing rechargeable lithium batteries. *Nature*. **414** (6861), 359-367 (2001).
2. Scrosati, B., Hassoun, J., & Sun, Y. Lithium-ion batteries. A look into the future. *Energy Environ. Sci.* **4** (9), 3287-3295 (2011).
3. Goodenough, J.B. & Kim, Y. Challenges for rechargeable batteries. *J. Power Sources*. **196** (16), 6688-6694 (2011).
4. Wang, Y., He, P., & Zhou, H. Olivine LiFePO₄: development and future. *Energy Environ. Sci.* **4** (3), 805-817 (2011).
5. Bruce, P.G., Scrosati, B., & Tarason, J. Nanomaterials for rechargeable lithium batteries. *Angew. Chem.* **47** (16), 2930-2946 (2008).
6. Choi, N., Yao, Y., Cui, Y., & Cho, J. One dimensional Si/Sn - based nanowires and nanotubes for lithium-ion energy storage materials. *J. Mater. Chem.* **21** (27), 9825-9840 (2011).
7. Jeong, G., Kim, Y.U., Kim, H., Kim, Y.J., & Sohn, H.J. Prospective materials and applications for Li secondary batteries. *Energy Environ. Sci.* **4** (6), 1986-2002 (2011).
8. Walker, C.W. & Salomon M. Improvement of ionic conductivity in plasticized PEO-Based solid polymer electrolytes. *J. Electrochem. Soc.* **140** (12), 3409-3412 (1993).
9. Daniels, C. & Besenhard, J.O. *Handbook of battery materials.*, Wiley-VCH GmbH & Co., Weinheim, 285 (2011).
10. Bard, A.J. & Faulkner, L.R. *Electrochemical methods: fundamentals and applications.*, 2nd ed., John Wiley and sons, New York, 864 (2001).
11. Newman, J. & Thomas-Alyea, K. *Electrochemical systems.*, 3rd ed., Wiley-Interscience, Hoboken, 672 (2004).
12. Zu, C. & Li, H. Thermodynamic analysis on energy densities of batteries. *Energy Environ. Sci.* **4** (8), 2614-2624 (2011).
13. Balbuena, P. & Wang, Y. *Lithium-ion Batteries: solid-electrolyte interphase.*, Imperial College Press, London, 424 (2004).
14. Appetecchi, G.B., Scaccia, S., & Passerini, S. Investigation on the Stability of the Lithium-Polymer Electrolyte Interface. *J. Electrochem. Soc.* **147** (12), 4448-4452 (2000).
15. Bruce, P.G. & Krok, F. Characterisation of the electrode/electrolyte interfaces in cells of the type Li/PEO LiCF₃SO₃/V₆O₁₃ by ac impedance methods. *Solid State Ionics*. **36** (3-4), 171-174 (1989).
16. Huggins, R. *Energy Storage*. Springer, New York, 400 (2010).
17. Lee, S., Schömer, M., Peng, H., Page, K.A., Wilms, D., Frey, H., Soles, C.L., & Yoon, D.Y. Correlations between ion conductivity and polymer dynamics in hyperbranched poly(ethylene oxide) electrolytes for lithium-ion batteries. *Chem. Mater.* **23** (11), 2685-2688 (2011).
18. Trapa, P.E., Reyes, A.B., Das Gupta, R.S., Mayes, A.M., & Sadoway, D.R. Polarization in cells containing single-ion graft copolymer electrolytes. *J. Electrochem. Soc.* **153** (6), A1098-A1101 (2006).
19. Trapa, P.E., Won, Y.Y., Mui, S.C., Olivetti, E.A., Huang, B., Sadoway, D.R., Mayes, A.M., & Dallek, S. Rubbery graft copolymer electrolytes for solid-state thin-film lithium batteries. *J. Electrochem. Soc.* **152** (1), A1-A5 (2005).
20. Walker, C.W. & Salomon, M. Improvement of ionic conductivity in plasticized peo-based solid polymer electrolytes. *J. Electrochem. Soc.* **140** (12), 3409-3412 (1993).
21. Bard, A.J., & Faulkner, L.R. *Electrochemical methods: fundamentals and applications.*, 2nd ed., John Wiley and sons, New York, 864 (2001).
22. Michnick, R.B., Rhoads, K.G., & Sadoway, D.R. Relative dielectric constant measurements in the butyronitrile-chloroethane system at subambient temperatures. *J. Electrochem. Soc.* **144** (7), 2392-2398 (1997).
23. Orazem, M.E., & Tribollet, B. *Electrochemical impedance spectroscopy*. John Wiley & Sons, Hoboken, 523 (2008).
24. Cogger, N.D., & Evans, N.J. *An introduction to electrochemical impedance measurement*. Technical Note, Solartron Analytical Technical Report No. 6, Part No. BTR006, Available for download at: <http://www.solartronanalytical.com/Literature/Technical-Notes.aspx>, (1999).
25. Marzantowiz, M., Dygas, J.R., & Krok, F. Impedance of interface between PEO:LiTFSI polymer electrolyte and blocking electrodes. *Electrochim. Acta*. **53** (25), 7417-7425 (2008).
26. Clarson, S.J., & Semlyen, J.A. Studies of cyclic and linear poly(dimethyl-siloxanes): 21. high temperature thermal behavior. *Polymer*. **27** (1), 91-95 (1986).